Improving the accuracy of single particle ICPMS for measurement of size distributions and number concentrations of nanoparticles by determining analyte partitioning during nebulisation

Journal of Analytical Atomic Spectrometry (ISSN: 0267-9477)

Citation for the published paper:
Tuoriniemi, J. ; Cornelis, G. ; Hassellöv, M. (2014) "Improving the accuracy of single particle ICPMS for measurement of size distributions and number concentrations of nanoparticles by determining analyte partitioning during nebulisation". Journal of Analytical Atomic Spectrometry, vol. 29(4), pp. 743-752.

http://dx.doi.org/10.1039/c3ja50367d

Improving Accuracy of Single particle ICPMS for Measurement of Size Distributions and Number Concentrations of Nanoparticles by Determining Analyte Partitioning During Nebulisation†

Jani Tuoriniemi[1], *Geert Cornelis*[1], *Martin Hassellöv*[1,*]

[1]Department of Chemistry and Molecular Biology, University of Gothenburg, SE-412 96 Gothenburg, Sweden

*CORRESPONDING AUTHOR: martin.hassellov@chem.gu.se, tel. +46-31-786 9050, fax +46-31-77227856.

†Electronic supplementary information (ESI) available.

TOC entry

The analyte is redistributed between the waste and plasma flows. These analyte partitioning effects need to be corrected for to obtain the most accurate size calibration of spICPMS.

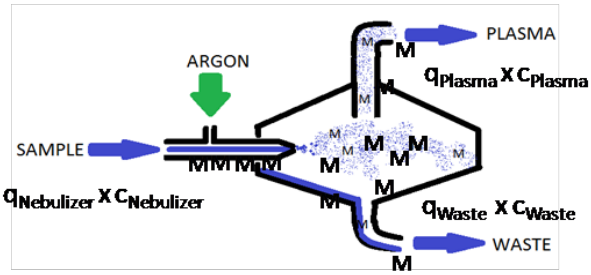

Abstract Application of single particle ICP-MS (spICPMS) for measurement of size and number concentration, c_p of nanoparticles is currently hampered by insufficient accuracy. The relative contributions of different types of noise to the overall uncertainty during spICPMS measurements of Ag and Au nanoparticle dispersions were quantified showing that the accuracy of spICPMS is mainly limited by the uncertainty in nebulization efficiency (f_{neb}). This uncertainty was improved by correcting f_{neb} for analyte partitioning effects during nebulization, and the calculated Ag and Au nanoparticle sizes were in close agreement with sizes determined by scanning electron microscopy. The duration of the particle events was measured, which allowed to correct for incomplete particle events, detector dead time, and to determine the effective dwell time for particle counting. The c_p measured with spICPMS agreed with that measured by counting particles deposited on filters, and calculated from the mass concentration of analyte.

Introduction The increased use of nanoparticles (NP) demands improved methods for their characterization.[1] Of particular concern is the lack of validated methods for measurement of particle number concentration, and number based size distributions in liquid samples at relevant concentrations.[2] Proposed EU legislation has adopted a particle number based definition of NPs. Enforcing regulations based on such definition would require accurate, sensitive and rapid particle counting techniques. These methods would find use in a range of applications such as environmental monitoring, characterization of samples for toxicological tests, industrial quality control, and improved characterization and studies of colloid dynamics.

Electron microscopy is time-consuming and is not capable of measuring particles in dispersion. Size fractionation with *e.g.* centrifugation or field flow fraction (FFF), followed by optical detection result in intensity weighted distributions that can be recalculated to number based ones, provided that the particles' optical properties are known. Such approaches are however limited to simple, and already well-characterized samples. Coupling FFF to techniques such as ICP-MS or ICP-OES[3] enables characterization of the mass as a function of, *e.g.*, hydrodynamic diameter of target inorganic nanoparticles in complex matrices. However, techniques for counting and sizing individual particles are required in order to also measure the number concentration, c_p.

The need for sensitive and selective methods for characterization of environmental colloids has led to development of single particle inductively coupled plasma mass spectrometry (spICPMS). When a particle enters the plasma it produces a burst of ions. If the dwell time is reduced to a level comparable to the duration of such pulses, the particle events appear as spikes in the continuous signal. It was shown by Degueldre *et al.*[4-8] and Laborda *et al.*[9] that the frequency of such spikes is proportional to the particle number concentration. The intensities depend on the mass of analyte in the particle. If the chemical composition is

known, the intensities can, provided suitable calibration, be calculated to spherical volume equivalent diameters. spICPMS can measure both size distributions and number concentrations of particles at extremely low concentrations (~10^2 particles mL^{-1}).[10] Since the technique is element-specific, particles of interest can be characterized in complex samples in the presence of orders of magnitude higher background particle concentrations, provided these particles consist of other elements. The measured diameters have been shown to be comparable to those measured using differential centrifugal sedimentation (DCS) analysis (Ag),[11] scanning electron microscopy (SEM) (SiO_2),[12] and nanoparticle tracking analysis (NTA) (Ag).[13] The number concentrations were in agreement with values calculated from mass concentrations of Au dispersions.[14] spICPMS has also potential to achieve an excellent size resolution because the mass of particles is proportional to the cube of their diameter.

To be able to develop spICPMS into a standard technique for regulations purposes it is necessary to identify the factors limiting its accuracy, because the particle size distributions analysed using spICP-MS are broadened relative to distributions analyzed with other techniques.[14] Therefore it was the aim of this study to evaluate the influence of parameters critical for both size and number concentration measurements, quantify the contributions of different types of noise affecting the size resolution, and to provide suggestions for further improvements.

One of the main factors limiting accuracy of both particle sizing and concentration determination is the uncertainty in the nebulization efficiency (f_{neb}).[10] It is the percentage of analyte, dissolved or nanoparticulate that is injected into the plasma. More than 80 % of the sample is redirected to waste from most conventional nebulizers, because the spray chamber only allows the finest droplets to reach the plasma, because these can be most easily dried, atomized and ionized. For conventional nebulizer-spraychamber systems, the only method for measuring the f_{neb} while the plasma is ignited is the waste collection (WC) method.[15] The

concentration of analyte ions in the aerosol droplets is lower in the vicinity of surfaces than in the bulk liquid. As the sample break up into droplets of decreasing size during the nebulization process, the smaller droplets that preferentially pass on to the plasma are formed primarily from this analyte depleted surface layer. These aerosol ion redistribution (AIR) effects[16] cause redistribution of the analyte between the waste and plasma flows so that the ratio of analyte to solvent in the stream going to the plasma is different than the ratio in the sample. The laborious procedure and disappointing results with the WC method have led to suggestions of using reference materials with known diameter, or number concentrations for determination of f_{neb}.[11] There are however neither reference materials with certified particle number concentrations nor validated methods for accurately measuring number concentrations for NPs. The use of reference materials with certified diameters adds cost and does not further the development of spICPMS into an independent method. In addition, any uncertainty in diameter is propagated cubed to the f_{neb}. For instance the ~ 5 % discrepancies among certified diameters for the NIST 60 nm Au particles would result in ~ 15 % uncertainty in f_{neb}.[11] It has also not been verified that nebulization efficiency is independent of the size and concentration of the reference nanoparticles. Validation and even modest improvements to f_{neb} determination methods are therefore likely to render spICPMS as accurate as many established particle sizing techniques.

In this article, methods to improve the accuracy of size distribution determinations using spICPMS or at least an alternative to presently used methods are presented. First, the magnitude of partitioning effects for the WC method are estimated by including dissolved In, and Au standards during waste collection. Correcting for dissolved analyte partitioning allows determining an analyte based f_{neb}[15] that takes AIR effects into account. The duration of particle events was measured using ultrafast acquisition times of 0.1 ms. It allowed estimation of the role of error sources such as incomplete measurement time and dead time error[12] at

higher acquisition times by computing the fraction of ions that are detected in each situation. Acquisition time is in this article referred to as dwell time (t_{dwell}). The levels of different types of noise in the particle signals are evaluated to estimate the resolution in particle sizes. The effective dwell time for particle counting is determined, and the combined effects of counting statistics, variation in particle flux, and uncertainty in f_{neb} for the accuracy of particle number concentration determination are discussed. The spICPMS c_p of Au colloids were compared with results obtained by counting particles on filters to assess the accuracy of particle number determination, and calculating it from the mass concentration and diameter. A list of symbols used in this article is found in table 1.

Experimental

Methods

Chemicals The citrate coated silver nanoparticles (AgNP) had a nominal diameter of 80 nm, and the also citrate stabilized gold nanoparticles (AuNP) were nominally 50, 100, and 250 nm (British biocell international, UK). Ultrapure water (Millipore MilliQ) was used as dilution media for all samples. Dissolved Ag, Au, and In standards were diluted from 1 gL^{-1} 2% HNO_3 solutions provided by Ultra Scientific in ultrapure water.

spICPMS A Thermo Element2 sector field ICP-MS was used in all experiments. The method, particle detection algorithm, and data acquisition of the used instrument are discussed in an earlier publication.[10] Data acquisition with 0.1 ms time resolution was achieved for the 80 nm Ag particles by using the following settings in the method file of the instrument software: Resolution: *low*, Samples per peak: *1000*, Integration window: *10*. As the instruments scans through the mass range set in the integration window, 100 consecutive dwells having 0.1 ms t_{dwell} are acquired without any time gap between them. The instrument parameters given in table 2 were optimized using dissolved In standards.

Determination of nebulization efficiency and calibrating for particle mass The nebulization efficiency was measured with 7 (Ag), and 8 (Au) replicates using the waste collection method.[15,10] Spray chamber waste flow (q_{waste}) was collected and weighted while the flow into the nebulizer ($q_{\mathrm{nebulizer}}$) was monitored using a flow meter (Glass Expansion ``truflow´´). The waste flow was driven by a peristaltic pump (Perimax 12). To investigate and correct for analyte partitioning between plasma and waste flows in the spray chamber, In (1μg L^{-1}) and Au (10 μg L^{-1}) was added to the sample flow and its concentration was measured both in the collected waste (c_{waste}), and inflow to the nebulizer ($c_{\mathrm{nebulizer}}$). The In concentration that effectively reaches the plasma (c_{plasma}) can be calculated from the mass-balance:

$$q_{\mathrm{plasma}}c_{\mathrm{plasma}} + q_{\mathrm{waste}}c_{\mathrm{waste}} = q_{\mathrm{nebulizer}}c_{\mathrm{nebulizer}} \quad (1)$$

The analyte-based nebulization efficiency f_{neb} then equals $c_{plasma} \times q_{plasma}(c_{nebulizer} \times q_{nebulizer})^{-1}$, whereas the more commonly used sample mass-based nebulization efficiency equals $q_{plasma}/q_{nebulizer}$. Note that in order to be able to calculate the analyte based f_{neb} it is enough to measure the ratio of the ICPMS signal intensities in the sample and collected waste. To calibrate for mass 0, 4, and 6 μg L^{-1} dissolved Ag standards and 1, 5, and 10 μg L^{-1}Au were measured using a dwell time of 10 ms.

Measurement of particle size distribution and concentration The AgNP stock dispersion was initially diluted 10^5 times using ultrapure water, and then further to a 10^7 times dilution in 20 replicates for size distribution and number concentration measurements. 10 000 consequent analyses (dwells) with a 10 ms t_{dwell} were measured on each replicate to obtain a total number of dwells (D) of 200 000, and to count 986 particle events. The Au particles were measured at 10^6 (50 nm), 10^5 (100 nm), and 10^4 (250 nm) times dilution and the number of particle events counted, N were 1250, 485, and 133 respectively. The total Au

concentrations in NP suspensions were measured in three replicates after digestion with *aqua regia*. To determine the effective dwell time and quantify bias due to incomplete particle events, the AgNP containing samples were diluted 1-2*10^6 times and were then measured using varying dwell times between 2 ms and 6 ms. In these experiments more than 500 particle events were counted for each dwell time.

To reduce the number of false positives, *i.e.* measurements of dissolved ions only that are recognized as particles, to a negligible level an iterative algorithm with an 8σ detection limit[10] was used for discriminating between particle events and the dissolved background. The mean value of the background signal was subtracted from the particle event signals. The signal intensity (I_{part}, ion counts) of a frequency-intensity diagram with bin width of 50 counts was recalculated to diameter, and the frequency (F,ND^{-1}) of the signals within each bin was recalculated to c_p using the formulas below.

$$d = [6(I_{part}\text{-}r)(\pi \rho s)^{-1}]^{1/3} \qquad c_p = F(f_{neb} t_{dwell} q_{nebulizer})^{-1} \quad (2)$$

r (ion counts) is the recipient on the intensity axis of the calibration curve, ρ is the density of the NP material, s is the sensitivity or slope of the calibration curve (ion counts g^{-1}).

Deposition of particles on filters The number concentrations of AuNP dispersions were measured by depositing the particles in a volume of dispersion on filters, and then using SEM to determine their surface concentration (particles m^{-2}). Knowing the total area of the filter that was exposed to the dispersion and the area that was imaged using SEM allowed calculation of the c_p (particles mL^{-1}) in the liquid sample. The Au colloids were diluted to 4*10^6 particles mL^{-1}, 9*10^7 particles mL^{-1}, and 6*10^9 particles mL^{-1} for the 250, 100, and 50 nm particles respectively. The filters were placed on glass frit supports giving an effective filtration area of 9.6 cm^2, and 10 mL of the dispersions were forced through by vacuum suction. The filters used for the 250 nm AuNP were the 100 nm nominal cut off cellulose

ester membranes from Millipore, while Corning 50 nm nominal cut off nuclepore track etched polycarbonate filters were used for the 100 and 50 nm samples. The experiments were performed in three replicates. The efficiency of retaining the particles was assessed by measuring total Au concentrations in the filtrate.

SEM A droplet of undiluted Ag colloid was placed on a silicon wafer, spread on the surface and left to dry in air. The sample preparation was done the same day as the spICPMS measurements. Secondary electron images with 40 000 – 50 000 times magnification were acquired with FEI quanta 200 FEG variable pressure SEM using 20 kV acceleration voltage. The Au particles were analyzed on the filters. A few small pieces were cut from each filter and placed on SEM stubs. Several backscattered electron images were taken at random locations on each piece, using again 20 kV acceleration voltage. The number of AuNP was counted in each image and the surface concentration was obtained by dividing with the imaged area. The instrument was operated in the high vacuum mode for Ag, while the non conducting filter substrates necessitated the use of low vacuum (~ 0.6 Torr) for imaging the Au particles.

For determining the surface concentration of AuNP, at least 700 particles were counted for each replicate. The magnifications were 3000 – 5000 times for the 100 and 250 nm AuNP, and around 20000 times for the 50 nm AuNP, except for some images used for counting only where ~ 8000 times magnification was sufficient. Images of the AuNP are shown in ESI-1.

Projected area diameters of 616 Ag particles were determined by fitting the particles with ellipses in the imageJ (National institute of health, http://imagej.nih.gov/ij) software. The automatic particle identification and sizing routine of the software was used to measure projected area diameters of 518, (50 nm), 531 (100 nm), 837 (250 nm) Au particles.

Results and discussion

Calibration for mass Uncertainties on numbers given are always 95% confidence intervals of the mean calculated from replicate measurements, unless stated otherwise. When measuring the Ag particles the f_{neb} based on sample mass was 6.7±2.2 %. The In concentration ratio between nebulizer ($c_{nebulizer}$) and waste flows (c_{waste}) was 0.76±0.14, resulting in an analyte-based f_{neb} of 4.7±1.8%. The Au particles were measured in a second session where the ratio of Au concentration between nebulizer and waste flows were 0.53±0.05 and the mass and analyte based f_{neb} were 8.7±0.49 %, and 4.7±0.26 % respectively. Dissolved analyte thus appear to partition preferentially to the waste. The AIR effects are not necessarily the same for NP as for dissolved analytes, but previous studies[17-18] found no significant differences when quantifying the total mass of NP with or without prior digestion. This suggests that dissolved analytes and NP similarly pass the sample introduction system. The nebulization efficiencies and size calibration parameters are listed in table 3.

Measurement of ion burst duration Data acquisition with 0.1 ms time resolution enabled to measure the durations of 16 particle events of 80 nm Ag (Fig. 1). The ion bursts appear to be Gaussian distributed as a function of time, with an average time-dependent standard deviation, σ_b of 0.08 ± 0.01 ms, but in many cases a tail could be observed because the cloud of ions expands while they are extracted through the sampler cone.[19] As 99.7% of the ions arrive within $3\sigma_b$ of the peak of the ion plume, $6\sigma_b$ can be used as a measure of the duration, t_b from the beginning to the end of the ion burst which is 0.48± 0.06ms.The duration of such ion plumes seems not to be dramatically different for varying materials and spectrometers, as in previous studies the t_b of ion bursts due to SiO_2 particles[12] were ~0.20-0.4 ms, while droplets containing dissolved analyte[20] gave bursts lasting between ~0.3 and 0.5 ms for the 20 different isotopes investigated, with a t_b of ~0.45 for silver.

SEM and spICPMS size distributions The majority of the Ag, and 50 nm Au particles were spheroidal (Fig. 2) with occasional rod- or triangular-shaped particles. The particles were

fitted with ellipses in order to calculate their projected area diameters. The average ratio of the major and minor axis of the particles was1.29, and 2.08 respectively, wherefore the projected area and volume equivalent diameters are not necessarily equal. The imaged AgNP were mostly part of aggregates. Care was taken to not measure particles that were obscured by their neighbors, since their diameters would appear smaller than their actual values. The spICPMS size detection limit, DL_s is the smallest ion burst that is distinguished as a particle event. The DL_s were 52, and 35 ion counts for the Ag and Au particles, which correspond to diameters of ~ 24 and 19 nm respectively. The DL_s for Ag is similar to that calculated in a previous publication.[10] The mean particle signals, I_{part} were 597, and 2017 ion counts for the Ag and Au particles respectively. The SEM and spICPMS size distributions are shown in Fig.3. For the AuNP, the spICPMS diameter obtained using analyte-based f_{neb} (61.06 nm) nearly coincided with the SEM diameter (63.48 nm), while the diameter seems to be overestimated using the mass-based f_{neb} (76.16 nm). For AgNP, the differences in diameters obtained by spICPMS using the analyte-based f_{neb} (56.24 nm), or the sample mass-based f_{neb} (60.74 nm) are smaller, and they are both in relatively close agreement with that calculated using SEM data, (61.99 nm).The accuracy of these size distributions are discussed further below. Note that the SEM size distribution of AuNP appears to be wider than that measured by spICPMS which is probably because of varying orientation of these asymmetric particles on the filter surface.

Accuracy of particle sizing A statistically significant number of particles were examined both with SEM, and spICPMS. The size distributions of the Au and Ag particles are by a good approximation Gaussian (r^2 of Gaussian fit is 0.96 and 0.95 for the Au and Ag particles respectively.). Therefore the uncertainty (95 % confidence interval) due to finite particle count can be approximated by $\pm 1.96 * e_{std}$, where e_{std} is the standard error of the mean diameter; $e_{std} = \sigma_{Size\ distribution} / (N)^{0.5}$. This uncertainty for spICPMS diameters (analyte-based

f_{neb}) were 0.32 nm and 0.57 nm for Ag and Au particles respectively, while it was 0.39 nm, and 1.54 nm for SEM.

The dwell time is one of the most important parameters in spICPMS. The intensity of a dissolved signal per dwell decreases when using a shorter t_{dwell}, but particle event intensities do not decrease. Decreasing the t_{dwell} thus increases the ratio between signals due to particles and dissolved analytes, allowing smaller particles to be detected. At the same time, the probability that a particle event does not completely coincide with t_{dwell} increases. The incompletely measured particle events broaden the distribution of particle signals and cause bias towards smaller particle sizes. However, when t_b is known, this error can be corrected for.

An average t_b = 0.48 ms was in this study obtained for 80 nm AgNP (Figure 1). The fraction of the ions from a particle event that is detected on average, f_d and the coefficient of variation for the spread in signal, $cv_{incomplete}$ is calculated as a function of dwell time in Fig. 4. It was assumed that the spread and bias are proportional to the signal intensity. The calculations were performed numerically by integrating the signal in a Gaussian having the same I_{part}, and t_b as obtained here in a moving window of width t_{dwell}. The distribution of signal intensities was obtained by sliding the window across the ion burst in steps of 0.001 ms. Such distributions were calculated both without assuming any detection threshold, and setting the DL_s to the values observed here. Experimental values are shown for a few different values of t_{dwell}. For this data, the f_d for 10 ms was assumed to be what was calculated, and f_d for shorter dwell times, t_{dwell} = x ms was calculated from $I_{part\ 10ms}/I_{part\ x\ ms}=f_{d10\ ms}/f_{d\ x\ ms}$. In the case of $DL_s=0$, and $t_{dwell}>t_b$ the f_d is given by (Derivation in ESI-2):

$$f_d=\frac{t_{dwell}}{t_{dwell}+t_b} \tag{3}$$

Eqn.3 is plotted in Fig.4. It agrees with the results obtained by numerical calculations for the case $DL_s = 0$. Fig.4 shows that f_d increases as t_{dwell} increases, because the change that the ion burst occurs completely within dwell increases. Eqn.3 can be used to correct for incomplete particle events, but as is evident in Fig.4, the bias is seemingly reduced with increasing DL_s as a larger fraction of the produced ions needs to be detected to exceed the detection limit, and a part of the incomplete particle events are thus not detected. Eqn. 3 under estimates f_d because the particle signals always need to exceed DL_s. However, the deviation from true values will be small for particle signals considerably higher than the DL_s. Because the variation in burst duration is small between different types of ions the calculations for Ag presented in Fig 4 are useful for estimating the bias for other analytes as well.

The incomplete particle events reduce the apparent particle mass of the Ag particles on average approximately ~3.1 % lower than its actual value when measured using a 10 ms dwell time. This reduces the calculated average diameter by ~ 1.2%.

Multiple particle event scan give rise to a spurious tail of large particles. However, according to Poisson statistics, only 0.234 % of the Ag particle events were due to more than one particle for the F of 0.00493. During a particle event the signal may momentarily reach high count rates while the automatic dead time correction is based on the average count rate during the whole duration of the dwell.[12] If 597 Ag ions are delivered as a Gaussian pulse with duration of t_b (σ=0.08ms), the average ion flux during the particle event will be 10^6 cps. Given that the detector has a dead time of 25 ns, only ~2.7 % of the ions are on average omitted from counting, resulting in ~ 0.9 % smaller size. For larger particles dead time could be a significant source of error, and it is advised that it should be evaluated for each measurement situation whether sensitivity should be reduced or if analogue ion detection is a more suitable option.

Finally, the error in f_{neb} is propagated to the *s*. The sensitivity can be can be rewritten as $I_{diss}(q_{nebulizer}t_{dwell}c_{nebulizer}f_{neb})^{-1}$, where the I_{diss} is the dissolved signal intensity. When this expression is substituted into Eqn 2 it becomes clear that the error is reduced to its third root when calculating the diameter. The percent uncertainty in particle diameter can be expressed as:

$$100\% \times \sqrt[3]{\frac{f_{neb} \pm \Delta f_{neb}}{f_{neb}}} = \Delta_{\%} d \quad (4)$$

In the case of Ag the 95% confidence interval in f_{neb} translates to an uncertainty in particle diameter ranging from -12.6 % to 10.0 %, and -15.1 % to 11.5 % for mass and analyte-based f_{neb} respectively. The uncertainty in nebulization efficiency is thus dominating source of error in these measurements, because other error sources are small or can be at least partially corrected for. The average particle diameter (analyte based f_{neb}) corrected for incomplete particle events and dead time becomes thus 57.4 with a 95% confidence interval ranging from 48.8 to 64.0 nm (Table 4). For comparison, the corresponding confidence interval for the diameter obtained with sample mass based f_{neb} without correction for analyte partitioning would be 53.1 – 66.8 nm. Regardless of if correction for analyte partitioning is applied or not, the SEM diameter is included in the confidence interval. The data do therefore not allow drawing any conclusions regarding the validity of the proposed correction scheme.

The data for AuNP demonstrates more clearly the feasibility of correcting for analyte partitioning. The frequency of multiple particle events is insignificantly low (1.3 % of the particle events), and the uncertainty in diameter due to f_{neb} is only ±~2 %. Correction for dead time and incompletely measured particle event error was also performed assuming that t_b is equal to that for Ag particles. The corrected diameter is equal to the size measured by SEM,

and has a confidence interval whose width is comparable to the accuracy of many established particle sizing methods[21] (Table 4).

Noise in particle signals The ability of spICPMS to resolve differing sizes is limited by the noise in particle signals. The standard deviation of particle event signals, σ_{total}, is due to both noise and polydispersity. It can be written as a sum of squares of its components:

$$\sigma^2_{\text{Polydispersity}} + \sigma^2_{\text{Ion Count}} + \sigma^2_{\text{Proportional}} + \sigma^2_{\text{Background}} + \sigma^2_{\text{Incomplete}} = \sigma^2_{\text{total}} \quad (5)$$

where $\sigma_{Ion\ count}$ is shot noise, *i.e.* the random error of the ion count. The signal during a particle event is the sum of ions originating from the particle, and those from the background levels of dissolved analyte. The mean intensity of background signal is subtracted from ion count to obtain I_{part} but its noise, $\sigma_{Background}$ remain in the particle signals. $\sigma_{Proportional}$ is flicker noise proportional to the signal intensity given by $\sigma_{Proportional} = I_{part} * cv_{pr,}$ where cv_{pr} is called the flicker factor. Flicker noise of dissolved ions is mainly caused by random sizes and arrival times of nebulized droplets, but also by varying trajectories of ions in the plasma and ion diffusion during transport from the plasma to the detector.[22] In the case of the noise on particle events, noise sources prior to atomization and ionization of particles in the plasma are irrelevant. The remaining flicker noise originates in varying trajectory lines of ions relative to the cone axis, and the distance from sampler cone to the point of vaporization and subsequently diffusion during transport to the detector.[23] The $\sigma_{Incomplete}$ is noise due incompletely measured particle events, $\sigma_{Incomplete} = I_{part} * cv_{Incomplete}$. The spread in particle signals increases sharply when t_{dwell} approaches the particle event duration (Fig.4).

The levels of different type of noise for the Ag particles are listed in table 5. For this sample any spurious spread in SEM size distribution is likely to be small, and $\sigma_{Polydispersity}$ was estimated by using Eqn. 2 to recalculate the SEM diameters to their corresponding I_{part} values. The $\sigma_{Background}$ was obtained from the signal variation in dwells where there were no

particles. The $\sigma_{Incomplete}$ was taken from Fig.4. To calculate $\sigma_{Ion\ count}$ it was assumed that this noise is given by $(\beta I_{part})^{0.5}$ where β is the shot noise coeficient.[24] The β was determined to 22.64 along with the flicker noise in dissolved signals in ESI-3. The remaining variation in particle signals was attributed to $\sigma_{Proportional}$.

The shot, flicker and noise due to incompletely measured particle events are dominating for these ~ 60 nm particles. The flicker noise appears to be smaller for particles (5.7 % RSD) than for dissolved analyte (10.2 % RSD). The background noise amplitude is most likely only quantitatively relevant close to the size detection limit. It is instructive to calculate the resolution in particle size to facilitate comparison with other methods. The resolution in particle mass, R_m can be defined as three times the standard deviation in I_{part} due to noise, which is divided by the sensitivity in order to convert the units to mass, $R_m = 3*\sigma_{noise}*s^{-1}$. For the Ag particles that are measured here the R_m is ~ 0.95 fg which corresponds to ~ 12 nm difference in diameter. This falls short from *e.g.* the sub nanometer resolution obtainable by analytical ultracentrifugation,[25] and the so far most sensitive suspended nano channel resonator device[26] that weighs Ag nanoparticles as small as 20 nm with an R_m of 0.027 fg. However, efforts to reduce the $\sigma_{Incomplete}$ by fast data acquisition[27] or correction using a known t_b as outlined above are likely to result in significant improvements in resolution.

Effective dwell time Decreasing t_{dwell} introduces also bias in particle number concentration. Large particles producing signals well above the DL_s may be detected even if the peak of the ion burst occurs a time t_p before the dwell starts, or after it ends. Fig.5 shows that the effective dwell time for determination of particle number concentration is in this case $t_{eff}=t_{dwell}+2t_p$. If more than 50 % of the ions produced by a particle needs to be detected for I_{part} to exceed DL_s; the peak of the ion burst must occur during a dwell (Fig.5). In this case the effective dwell time becomes shorter than the set dwell time, *i.e.* t_p becomes negative. For the Ag particles

investigated here, an average t_p of 0.15 ms was calculated from I_{part}, $t_{b,}$ and DL_s. An experimental value was determined using a procedure developed by Heithmar.[28] Using $t_{dwell} + 2t_p$ instead of $t_{dwell,}$ equation 2 can be rearranged to:

$$\frac{F}{c_p} = f_{neb} q_{nebuliser} t_{dwell} + 2t_p f_{neb} q_{nebuliser} \quad (6)$$

In Fig. 6 Fc_p^{-1} is plotted against t_{dwell}, and a t_p of 0.31±0.24ms is obtained by dividing the intercept ($2t_p f_{neb} q_{nebuliser}$) with the slope ($f_{neb} q_{nebuliser}$) using equation (6). The confidence interval magnitude expresses the uncertainty in the fit parameters, a value that is high because the value of the intercept is sensitive to random error in F that scatters the data points. This method should consequently be used with caution.

Accuracy of particle number concentration determination The random uncertainty in c_p, $\Delta c_{p\ Random}$ is given by the root sum of squares of the counting statistics confidence interval, $\Delta c_{p\ Particle\ count}$ and uncertainty in nebulization efficiency, $\Delta c_{pf_{neb}}$. It is also possible that the particle frequency is not constant during the measurements due to *e.g.* fluctuations in sample flow rate. In this case uncertainty due to short term fluctuations in F, Δc_{pF} should also be taken into consideration.

To calculate the $\Delta c_{p\ Particle\ count}$ it is assumed that the number of particles that are detected in a sequence of D dwells with a particle frequency $F=ND^{-1}$ is given by the binomial distribution. For such distribution, there exists several ways of approximating the confidence interval in F as a function of F and D.[29] The fact that N is given by $N=DF$ allows to express these confidence intervals as a function of particle count. An approximation for the ΔF as function of particle count was derived previously using the Wald confidence interval.[10] Here the more reliable Wilson confidence interval was used instead, because the confidence intervals calculated by the Wald equation may be significantly shorter than their true values for small

values of D.[29] An approximation to the relative width of the 95 % confidence interval, ΔFF^{-1} as a function of N was calculated according to equation 4 in Ref.29, and shown in Fig7.

To investigate if there were significant fluctuations in F, a bootstrap method[30] was applied to estimate the uncertainty as a function of N based on experimental data. Dwells were chosen randomly with repetition and inspected for particle events from the set of 200 000 measured dwells. This was repeated D^* times, until the desired number of particle events were found. 2000 D^* values were acquired, and a 95% confidence interval for D^* was calculated by ordering the set of D* and considering the values of the 100: th and 1900: th elements as the confidence interval boundaries. The confidence interval in D^* is for a given particle frequency proportional to the uncertainty in c_p, which is here denoted $\Delta c_{p\ Bootstrap}$. The relative width of $\Delta c_{p\ Bootstrap}$ is shown as a function of N in Fig. 7.

The $\Delta c_{pParticle\ count}$ and $\Delta c_{p\ Bootstrap}$ follow each other closely; however the bootstrap technique seems to slightly underestimate the width of the confidence interval for most values of N. Note also that the bootstrap confidence interval does not follow a smooth curve due to the random nature of the calculations. These results suggest that the contribution from Δc_{pF} was not significant here. The total random uncertainty is therefore given by:

$$\Delta c_{pRandom} = \sqrt{\Delta^2 c_{pParticle\ count} + \Delta^2 c_{pf_{neb}}} \qquad (7)$$

The relative width of $\Delta c_{p\ Random}$ is plotted in figure 7. The random uncertainty in this case decreases initially rapidly with increasing particle count to reach a level determined mainly by $\Delta c_{pf_{neb}}$ at ~300 particle events. The c_p in the Ag dispersion was measured to 528 particles mL^{-1} with a 95 % confidence interval ranging from 380 to 976 particles mL^{-1} using the calculated t_{eff} of 10.3 ms. Correction for effective dwell time is unlikely important when using 10 ms t_{dwell}, because t_{eff} is not more than a few percent longer than the set dwell time. The

relative importance of dwell time correction increases for shorter dwell times, and when t_{dwell} approaches the duration of the ion burst (t_{dwell}~ <2 ms) it might become significant in comparison with the random error.

To evaluate the magnitude of non random error, the number concentrations of AuNP measured by spICPMS are compared in Fig.8 with those measured by counting particles on filters (Filter deposition), and calculated from analyte mass concentration and diameter assuming a spherical shape (Total Au mass). The SEM diameters, aspect ratios, and concentrations measured by spICPMS are listed in table 6. Note that the sizes for 100 and 250 nm AuNP differ significantly from their nominal values. This is probably due to Ostwald ripening because these dispersions were old. After using the bootstrap method to confirm that there were no significant fluctuations in F, the uncertainties in c_p were calculated according to Eqn. 7and are shown in Fig. 8. The frequencies of multiple particle events were not significant for the larger AuNP either, with 0.47 %, and 0.13 % of the particle events for 100 nm, and 250 nm AuNP being due to more than one particle.

The c_p calculated from mass concentration is not necessary equal to the true value because these particles are not completely spherical. Based on analysis of the filtrate, more than 99.99 % of the mass of Au in the 250, and 100 nm dispersions, and 91 % of that in the 50 nm dispersions were retained on the filters. However, the accuracy of the filter deposition method is reduced due to aggregation, and because the examined areas are not necessarily fully representative as the surface concentration varied over the filter area.

The shortcomings of the methods of comparison result in a large spread in the c_p values, that nevertheless agree relatively well with spICPMS. The average ratio of reference c_p, and spICPMS c_p for each of the 6 reference values for the three samples was1.27±0.64. More accurate reference methods are required to assess subtle error sources such as analyte

partitioning, off axis trajectories of particles in plasma, and adsorption of particles to tubing and container walls.

Conclusions and outlook The accuracy of both particle diameter and c_p are ultimately limited by the uncertainty in f_{neb}. It was found that systematic errors in the WC method could be significantly reduced by correcting f_{neb} for analyte partitioning between plasma and sample flows, however further work is necessary in order to develop this approach into an fully reliable analytical method. Among other things, it should be investigated whether size fractionation occurs in the spray chamber. The other identified error sources are small, and can be at least partially corrected for, if proper care is taken during measurements. If f_{neb} would be known precisely, the sizing accuracy of spICPMS would rival *e.g.* the 3 % achievable by electrospray scanning mobility particle sizer (ES-SMPS),[31] and the 5 % accuracy of magnification calibration in SEM, which is nominally reached by following American society for testing materials (ASTM) standard procedures.[32]

The size resolution is limited by the noise in particle signals. The noise in particle signals is dominated by that due to shot, incomplete particle events, and flicker noise, which could be reduced by proper measurement settings and sample introduction respectively. For instance, when measuring ion bursts from a train of droplets containing dissolved analyte introduced by a monodisperse dried microparticle injector (MDMI) device and acquiring data with fast time resolution using an oscilloscope, the coefficient of variation was reduced to 5 %.[19] However, the magnitudes of noise in the measurements made in this article are still low enough for polydispersity to dominate the spread in sizes for most samples that are encountered in practice.

No systematic bias in number concentration that exceeds the margin of uncertainty of the reference methods was observed. Further improvements in accuracy of spICPMS in terms of

particle counting are difficult due to the lack of accurate and validated reference methods. Counting particles on filters could be developed to such high accuracy technique. Particle populations can be quantitatively retained on filters, and if filtration devices utilizing small enough filter areas (< 1 mm^2) were used, sampling error could be eliminated by counting all of the particles in a volume of dispersion. The aggregation on filter surfaces could be reduced by decreasing the concentration in the filtered dispersion.

A completely different approach to determine f_{neb} would be to add particles quantifiable by optical means to the sample flow. An accurate method for particle counting using fluorescence spectrometry is being developed for micron sized particles.[33] If it could be extended to fluorescent quantum dots, rapid and accurate determination of a particle based f_{neb} would be possible by passing the sample flow through a fluorescence detector. Besides the possibility to create an internal standard for nebulization efficiency, such hyphenated system would allow straight forward quantification of possible losses due to adsorption on surfaces and trajectories lying off the sampler cone axis.

SUPPLEMENTARY INFORMATION Electronic supplementary information (ESI) is available as indicated in text.

ACKNOWLEDGEMENT

We thank the following funding agencies for support: European Commission FP7 projects NANOFATE (Ref#: 247739, 2010-2014) and MARINA (Ref#: 263215, 2011-2015), the Swedish Environmental Research Council FORMAS and the Gothenburg graduate school Environment and Health.

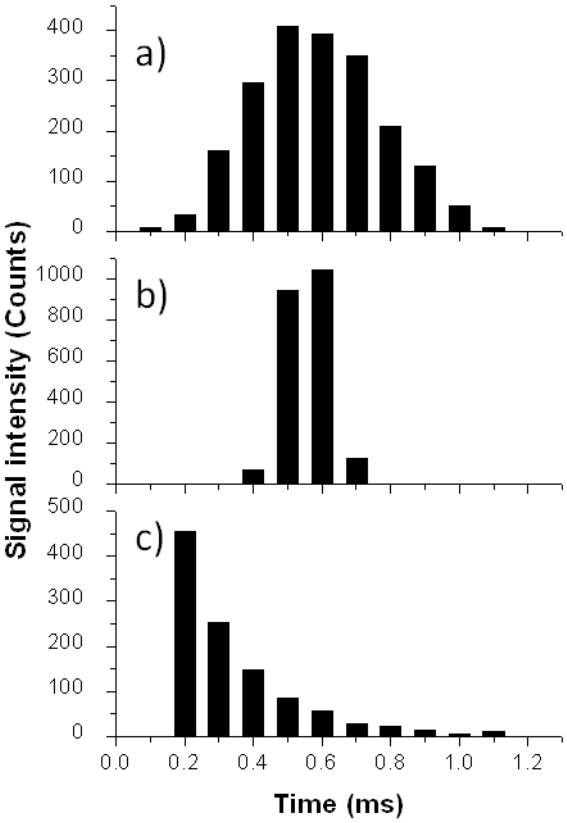

Fig. 1 Particle events of 80 nm Ag particles measured using fast data acquisition with 0.1 ms time resolution. a) A particle event that is a) broader, and b) narrower than average. c) An extreme case of the occasionally observed tailing effect.

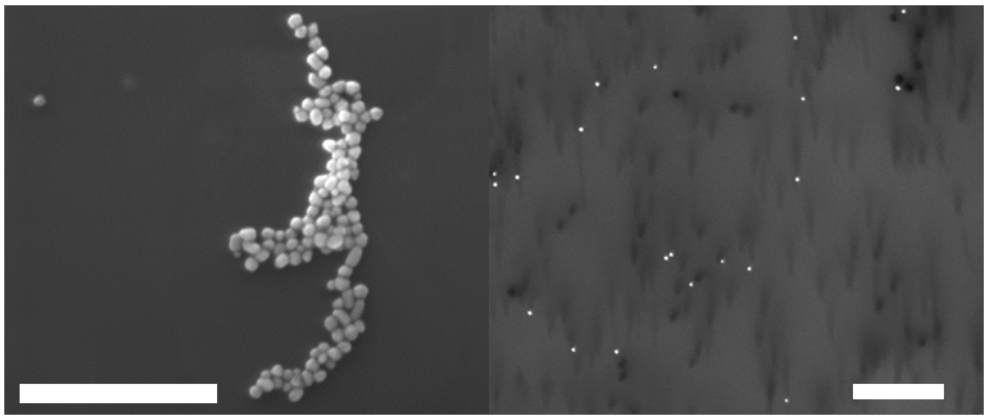

Fig. 2 Images of 80 nm AgNP (Left), and 50 nm AuNP (Right). The scale bars are 1 μm.

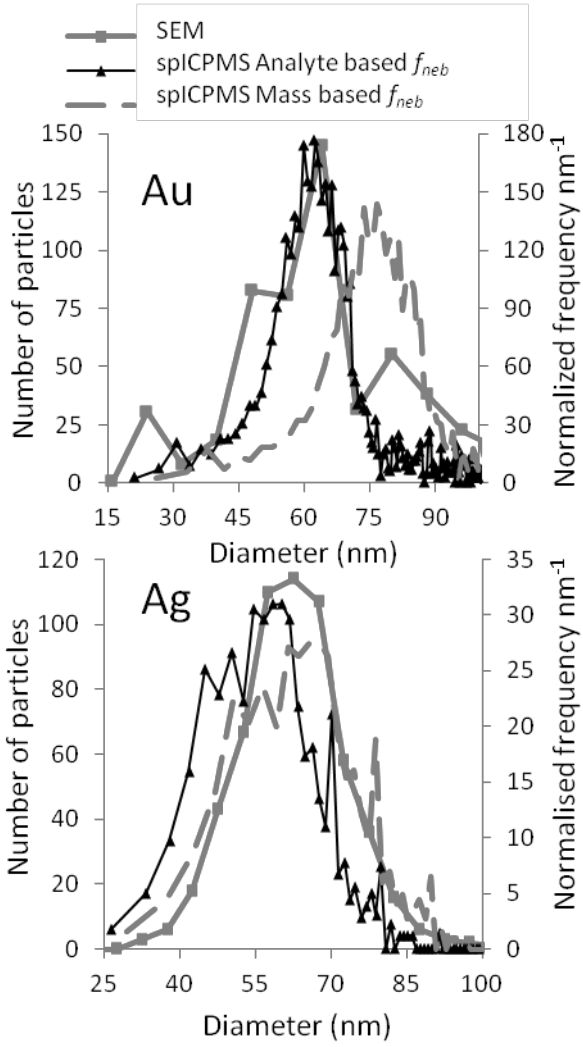

Fig.3 SEM and spICPMS size distributions of the 80 nm AgNP and 50 nm AuNP. The spICPMS size distributions were calculated using both mass and analyte based f_{neb}.

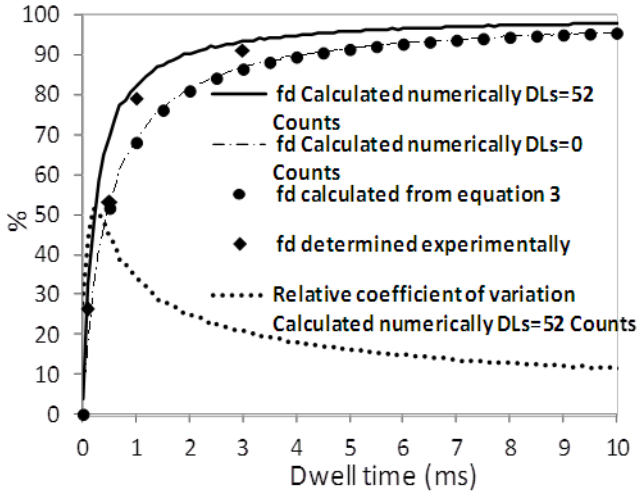

Fig.4 The average fraction of ions in the particle events with an ion burst duration t_b = 0.48 ms that are appearing in each dwell, f_d, as a function of dwell time for both theoretical and experimental data. Theoretical calculations using two different size detection limits are shown. The relative coefficient of variation (spread) of particle signal intensities due to incomplete particle events is also included.

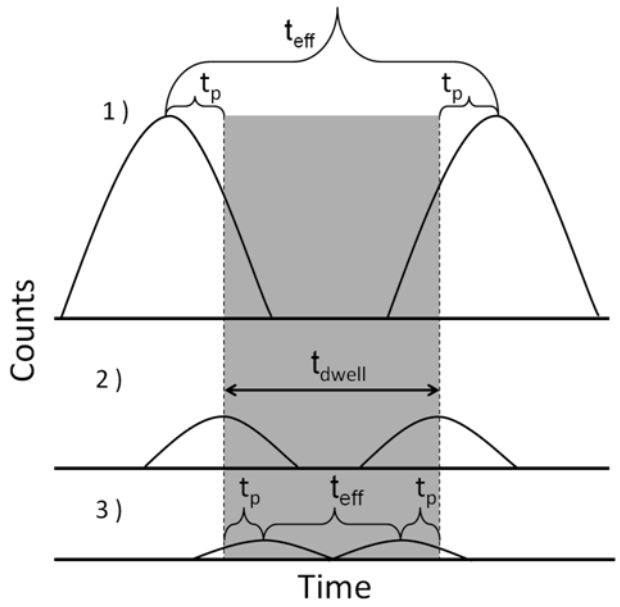

Fig.5 Illustration explaining the concepts particle time, t_p effective dwell time, t_{eff}, and set dwell time, t_{dwell}. 1) The effective dwell time is longer than t_{dwell} for a large particle where only the tails of ion bursts need to coincide with the dwell time for it to be detected. 2) When half of the ions have to be detected to exceed the detection threshold, DL_s, the t_{eff} is equal to the set dwell time.3) In order to detect a small particle, most of the ions must arrive during t_{dwell}. In this case, the effective dwell time for particle detection becomes shorter, *i.e.* t_p is negative.

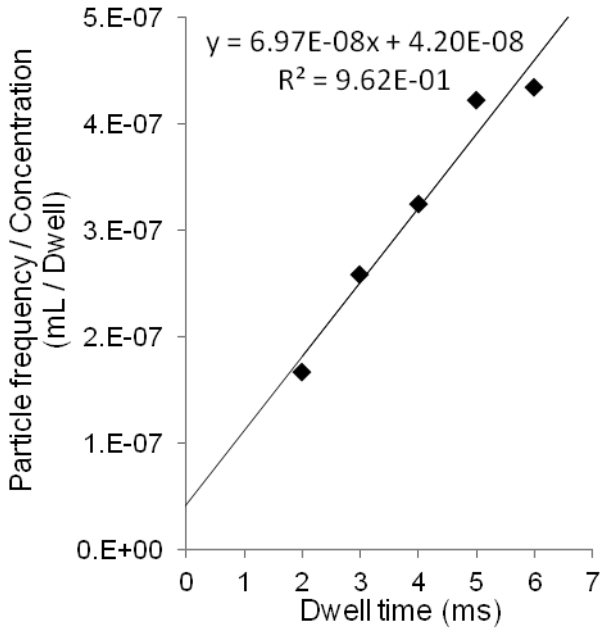

Fig.6 The concentration normalized particle frequency as a function of dwell time. The slope and intercept of the fitted line was used for determination of t_{eff}.

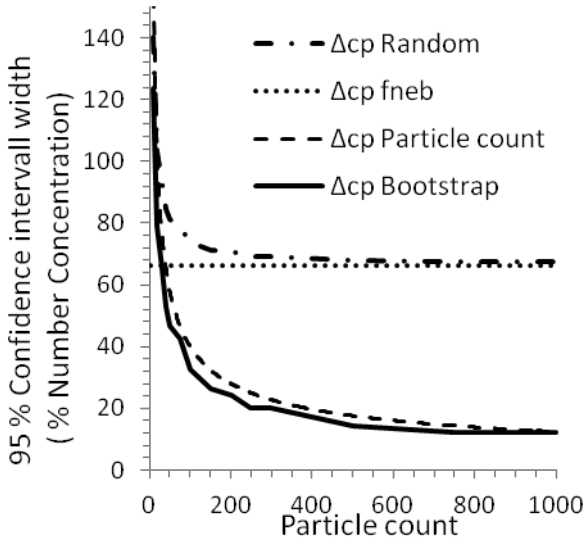

Fig.7 The width of confidence intervals of c_p as a function of particle count: The confidence interval of c_p due to total random uncertainty calculated from Eqn. 7 ($\Delta c_{p\ Random}$).The confidence interval of c_p due to the uncertainty in f_{neb} ($\Delta c_{pf_{neb}}$). The Wilson confidence interval of c_p due to counting statistics ($\Delta c_{p\ Particle\ count}$).The uncertainty calculated using the bootstrap method ($\Delta c_{p\ Bootstrap}$).

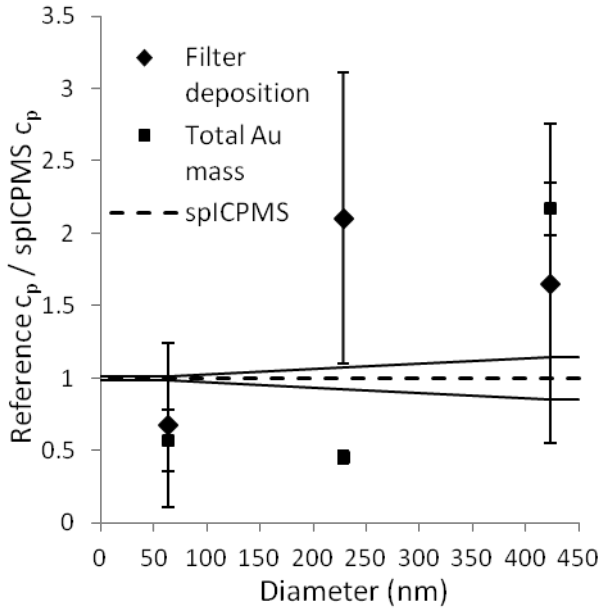

Fig.8 The ratio of number concentrations measured by the reference methods and spICPMS. The lines indicating spICPMS error show the uncertainty due to inaccurate nebulization efficiency, and stochastic error in particle count determined according to equation 7. The uncertainty for the filter counting data is due to variation among replicate experiments, while that of the analyte mass is due to combined effects of uncertainty in particle diameter, and variation among replicate ICPMS measurements.

Table 1. List of symbols.

Symbol	
$\mathbf{c_p}$	Number concentration (Particles V^{-1})
D	Number of dwells
N	Number of particles
F	Particle frequency ($N\ D^{-1}$)
$\mathbf{DL_s}$	Detection limit (Counts)
$\mathbf{I_{part}}$	Particle signal intensity (Counts)
$\mathbf{I_{diss}}$	Dissolved signal intensity (Counts)
s	Sensitivity (Counts g^{-1})
q	Flow rate ($V\ s^{-1}$)
c	Concentration (gV^{-1})
$\mathbf{f_{neb}}$	Nebulization efficiency (%)
Δ	Confidence interval
$\boldsymbol{\sigma}$	Standard deviation
$\mathbf{t_{dwell}}$	Dwell time (s)
$\mathbf{t_b}$	Duration of ion burst (s)
$\mathbf{t_p}$	Particle time (s)
$\mathbf{t_{eff}}$	Effective dwell time (s)
cv	Coefficient of variation (RSD %)
$\mathbf{f_d}$	Fraction of ions measured

$\mathbf{R_m}$	Resolution in particle mass (g)
d	Particle diameter (m)
$\boldsymbol{e_{std}}$	Standard error of the mean (m)

Table 2. Masspectrometer tune parameters and sample introduction components.

Sample gas flow rate (L min^{-1})	~1.370
Auxiliary gas flow rate (L min^{-1})	~0.96
Cool gas flow rate (L min^{-1})	15.02
Sample uptake rate (ml min^{-1})	~0.523
RF power (W)	1158
Nebulizer	Micromist 0.4 ml/min uptake rate concentric nebulizer (Glass expansion)
Spray chamber	Cyclonic (Glass expansion)
Torch	Fassel type (Thermo Finnigan)
Sample cone	Nickel 1.0 mm orifice diameter
Skimmer cone	Nickel 0.8 mm orifice diameter

Table 3. Nebulization efficiency and particle size calibration parameters.

Sample	$\boldsymbol{q_{nebulizer}}$	$\boldsymbol{q_{waste}}$	***Mass based*** $\boldsymbol{f_{neb}}$	***Analyte based*** $\boldsymbol{f_{neb}}$	***Sensitivity***	***Recipient***
Ag 80 nm	0.53 ±0.012 mL / min	0.49 ± 0.017 mL / min	6.7±2.2 %	4.7±1.8 %	$4.99*10^{17}$ Counts g^{-1}	123 Counts
Au 50 nm	0.56±0.0055 mL / min	0.51± 0.0037 mL / min	8.7±0.49 %	4.7±0.26 %	$5.08*10^{17}$ Counts g^{-1}	739 Counts

Table 4. SEM and spICPMS diameters of AgNP, and 50 nm AuNP showed together with the magnitudes of bias and uncertainty in the spICPMS measurements. The spICPMS diameters were corrected for bias, and the corrected values are given with the 95 % confidence interval due to Δf_{neb}.

Particles	spICPMS *d*[†]	Dead time[‡]	Incomplete particle events[‡]	Δf_{neb}	Corrected spICPMS *d*	SEM *d*
AgNP	56.24 nm	-0.9 %	-1.2 %	-15.1 % +11.5 %	48.8 - 64.0 nm	61.99 ±0.39 nm
50 nm AuNP	61.06 nm	-3.3 %	-1.2 %	-1.9 % +1.8 %	62.6 - 65.0 nm	63.48 ±1.54 nm

[†] Measured using analyte based f_{neb}. [‡]It was assumed that the t_b of Au particles equaled that measured for Ag.

Table 5. Contributions of sample polydispersity and noise to the spread in particle signals (Relative standard deviation, RSD).

$\sigma_{Polydispersity}$[†]	$\sigma_{Ion\ Count}$	$\sigma_{Proportional}$	$\sigma_{Incomplete}$[‡]	$\sigma_{Background}$	σ_{total}
51 % RSD	18.9 % RS	5.7 %RSD	12 % RSD	1 % RSD	56 % RSD

[†]Determined from SEM data. [‡] The contribution from incomplete particle events was estimated from figure 4.

Table 6. Properties of the AuNP dispersions.

Sample	Aspect ratio	SEM diameter[†]	spICPMS Concentration[‡]
Au 50 nm	2.08	63.48±1.54 nm	5631particles mL^{-1}
Au 100 nm	1.58	228.1±16 nm	2185 particles mL^{-1}
Au 250 nm	1.68	423.0±13.6 nm	599 particles mL^{-1}

[†]The uncertainty was calculated from the e_{std}. [‡]The concentration in the dispersions diluted for measurement.

References

1. P.J.J. Alvarez, V. Colvin, J. R Lead, V. Stone, *ACS Nano* 2009, **3**,1616-1619
2. K. Ehara, H.Sakurai, H, *Metrologia* 2010, **47**, S83-S90

3. S. Dubascoux, I. L. Hecho, M. Hassellov, F. V. D. Kammer, M. P. Gautier. G. Lespes, *J. Anal. At. Spectrom.* 2010, **25**, 613-623.

4. C. Degueldre, P. Y. Favarger, *Colloids Surf. A* 2003, **217**, 137-142.

5. C. Degueldre, P. Y. Favarger, *Talanta*, 2004, **62**, 1051-1054.

6. C. Degueldre, P. Y. Favarger, C. Bitea, *Anal. Chim. Acta*, 2004, **518**, 137-142.

7. C. Degueldre, P. Y. Favarger, S. Wold, *Anal. Chim. Acta*, 2006, **555**, 263-268.

8. C. Degueldre, P. Y. Favarger, S. Wold, *Talanta*, 2006, **68**, 623-628.

9. F. Laborda, J. Jimenez-Lamana, E. Bolea, J. R. Castillo, *J. Anal. At. Spectrom.* 2011, **26**, 1362-1371.

10. J. Tuoriniemi, G. Cornelis, M. Hassellöv, *Anal.chem.* 2012, **84**, 3965-3972.

11. H. E. Pace, N. J. Rogers, C. Jarolimek, V. A. Coleman, C. P. Higgins, J. F. Ranville, *Anal.chem.*2011, **83**, 9361–9369

12. J. W. Olesik, P. J. Gray, *J. Anal. At.Spectrom.*2012, **27**, 1143-1155

13. H. E. Pace, N. J. Rogers, C. Jarolimek, V.A. Coleman, C. P. Higgins, E. P. Gray, J. F. Ranville, *Env. Sci. Tech.*2012, **46**, 12272–12280.
14. F. Laborda, J. Jimenez-Lamana, E, Bolea, J.R. Castillo, *J. Anal. At. Spectrom.* 2013, **28**, 1220-1232.
15. D. Smith, R. Browner, *Anal.Chem.*1982, **54**, 533-537.

16. J. A. Boroweic, A. W.Boorn, J. H. Dillard, M. S. Cresser, R. F. Browner, *Anal. Chem.* 1980, **52**, 1054-1059.
17. D. M. Mitrano, E. K. Lesher, A. Bednar, J. Monserud, C. P. Higgins, J. F. Ranville, *Environ.Toxicol.Chem.* 2012, **3**, 115–121.
18. R. Allabashi, W. Stach, A. de la Escosura-Muniz, A. L. Liste-Calleja, A. Merkoci, *J. nanopart. Res.* **2009**, 11, 2003-2011.

19. I. I.Stewart, J.W. Olesik, *J. Am. Soc. mass spec.*1999, **10**, 159-174.

20. O. Borovinskaya, B. Hattendorf, M.Tanner, S. Gschwind, D. Günther, *J. Anal. At.Spectrom.* 2013, **28**, 226-233.

21. A. Lamberty, K. Franks, A. Braun, V. Kestens, G. Roebben, T. P. J. Linsinger, *J. nanopart.Res.* 2011, **13**, 7317–7329

22. J.W. Olesik, J. A. Kinzer, G. J. McGowan, *Appl.Spectrosc.*1997, **51**, 607-617.

23. M. P. Dziewatkoski, L.B. Daniels, J.W. Olesik. *Anal.Chem.*1996, **68**, 1101-1109.

24. G. Cornelis, M. Hassellöv, *J. Anal. At. Spectrom.* 2013 Accepted for publication **DOI:** 10.1039/C3JA50160D

25. K. L. Planken, and H. Cölfen, *Nanoscale,* 2010, **2**, 1849-1869.

26. J. Lee, W. Shen, K. Payer, T. Burg, S. Manalis, *Nano lett*2010, **10**, 2537–2542

27. S. Gschwind, L. Flamigni, J. Koch, O. Borovinskaya, S. Groh, K. Niemax, D. Gunther, *J.Anal. At.Spectrom.* 2011, **26**, 1166-1174.

28. E. M. Heithmar, *237th ACS National meeting*; abstracts of papers of the American chemical society: Salt lake city, UT USA, **2009**; Vol. 237, pp 58-COLL

29. L.D. Brown, T.T. Cai, A. DasGupta, *Stat.Sci.,* 2001, **16,** 101-133.

30. J. Carpenter, J. Bithell, *Statist. Med.* 2000, **19**, 1141-1164.

31. D. P. Kinney, D. Y. HPui, G. W. Mulholland, N.P. Bryner, *Journal of Research of the National Institute of Standards and Technology* 1991,**96**, 147-176.

32. ASTM E766:98 American society of testing materials **2008**

33. T. Sakaguchi, K. Ehara, *Proceedings SPIE* 5856 *Optical Measurement Systems for Industrial Inspection IV*, 994 (August 03, 2005); **DOI**:10.1117/12.612472

Improving Accuracy of Single particle ICPMS for Measurement of Size Distributions and Number Concentrations of Nanoparticles by Determining Analyte Partitioning During Nebulisation

SUPPLEMENTARY INFORMATION

Jani Tuoriniemi[1], *Geert Cornelis*[1], *Martin Hassellöv*[1,*]

[1]Department of Chemistry and molecular biology, University of Gothenburg, SE-412 96 Gothenburg, Sweden

[*]CORRESPONDING AUTHOR: martin.hassellov@chem.gu.se, tel. +46-31-786 9050

Table of Contents

ESI-1 SEM images of particles deposited on filters

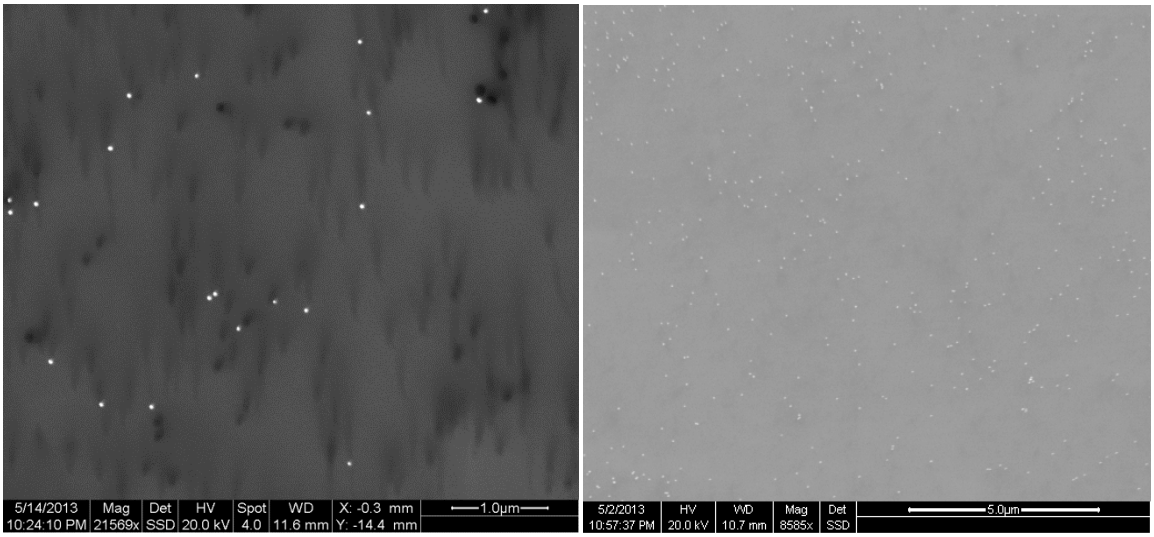

Figure S-1 50 nm AuNP deposited on a filter. Left: a high magnification (21569 X) BSE image used for particle sizing. Right: A low magnification (8585 X) BSE survey image for particle counting.

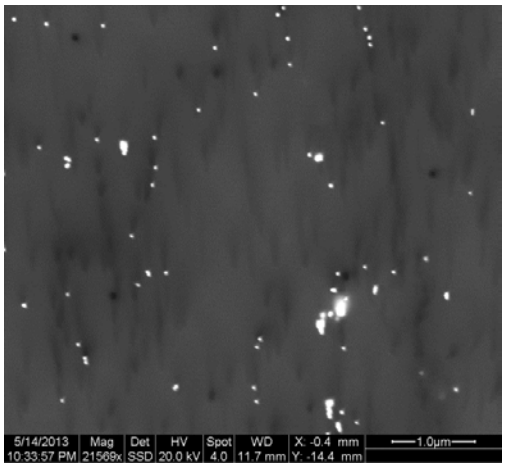

Figure S-2 50 nm AuNP deposited on filter. (BSE, 21589 X magnification). The particles tended to occasionally aggregate on the surface, as can be seen in the above image.

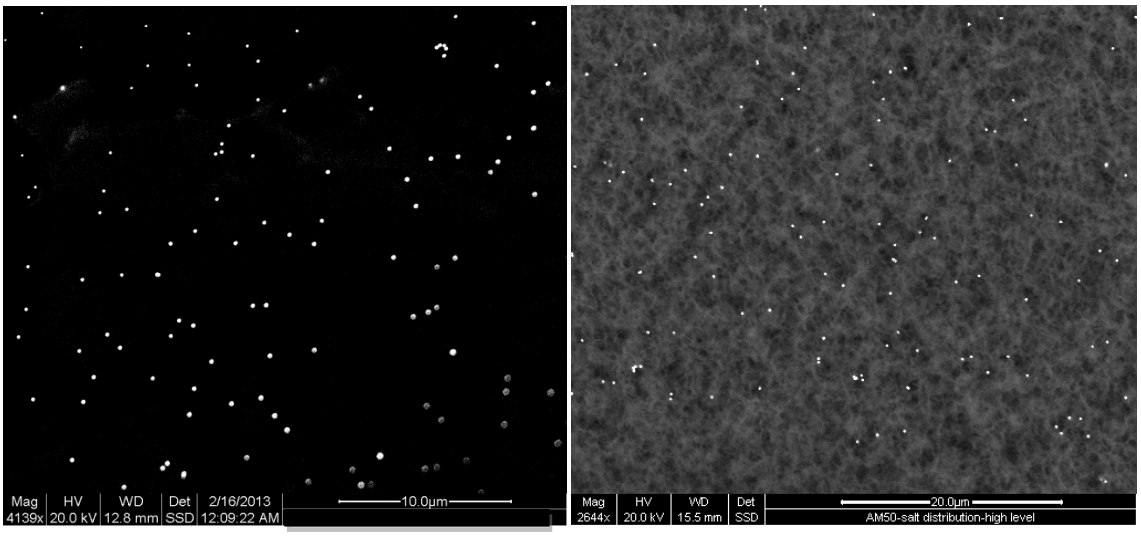

Figure S-3 BSE images of: Left) 100 nm AuNP on filter, 4139 X magnification, Right) 250 nm AuNP, 2644 X magnification. These images were used both for particle sizing and counting.

ESI-2 Derivation of equation for estimation of error in particle mass due to incomplete particle events

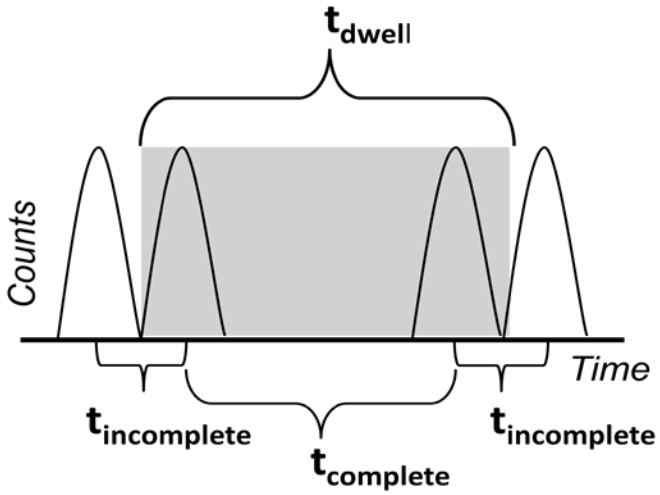

Figure S-4 The time intervals during which particle events become completely and incompletely measured.

The above figure illustrates the times during which an ion burst becomes comes completely and incompletely measured. If it is assumed that there is no signal intensity threshold for detecting a particle event, *i.e.* $DL_s=0$, particles may be detected even if the peak of an ion

burst occurs a time ½ t_b (duration of ion burst) before a dwell starts or after it ends. However, in order for the particle event to be completely measured the particles must arrive ½ t_b after the dwell starts or before it ends. For each dwell there is thus a time period of $2t_b$ during which an incoming ion burst may become only partially detected, $t_{incomplete}$; and a period of duration t_{dwell} -t_b during which all ions are detected completely, $t_{complete}$. As the particles are assumed to arrive at random times, the fraction of particle events that are incompletely measured, F_i is given by ratio of $t_{incomplete}$ and the total time for particle detection given by the sum of $t_{incomplete}$ and $t_{complete}$:

$$F_i = \frac{2t_b}{t_{dwell} + t_b} \qquad \text{(SI-1)}$$

The equation is valid for $t_{dwell} > t_b$, since for shorter t_{dwell} no particle events become completely measured. It can be assumed that the measured signal of an incomplete particle event, $I_{incomplete}$ is on the average half of the complete particle signal, I_{part}, i.e. $I_{incomplete} = ½ I_{part}$. The average signal due to complete and incomplete particle events, I_{avg} is then given by:

$$I_{avg} = I_{part}(1 - ½F_i) \qquad \text{(SI-2)}$$

An expression for the fraction of I_{part} that on average becomes measured f_d , $f_d = I_{avg}/I_{part}$, is obtained by combining equations SI-1 and SI-2 to:

$$f_d = \frac{t_{dwell}}{t_{dwell} + t_b} \times 100\ \% \qquad \text{(SI-3)}$$

ESI-3 Determination of noise in dissolved Ag signal.

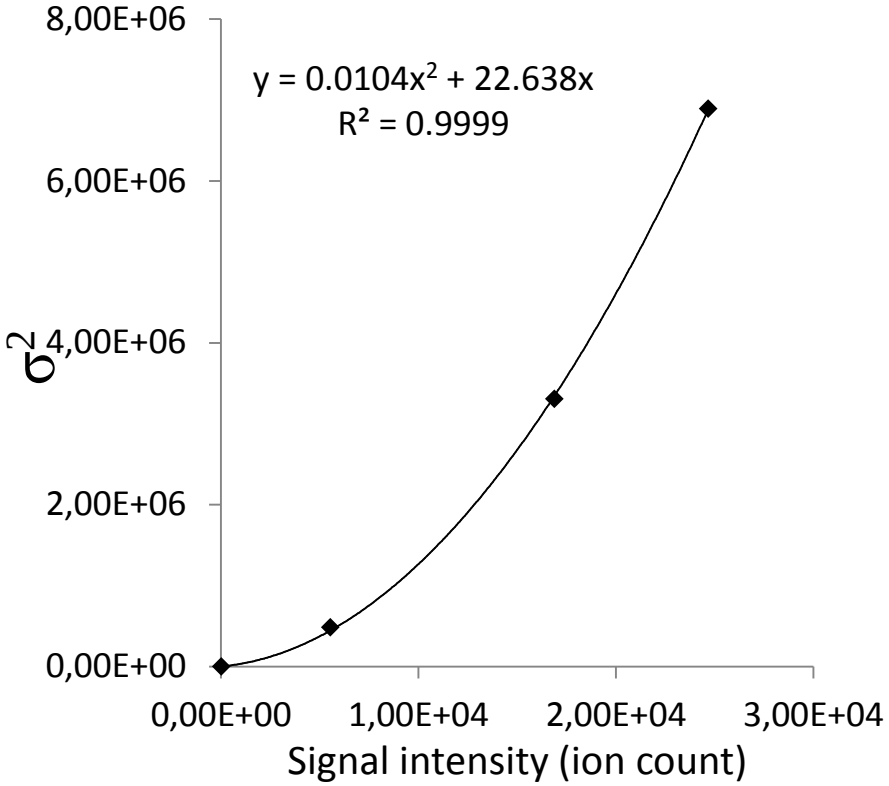

Figure S-5 The square of the standard deviation of dissolved Ag signal as a function of signal intensity.

The noise in signal originating from dissolved ions, σ_I can be assumed to be composed of flicker noise proportional to the signal intensity, I and shot noise given by $(\beta I)^{0.5}$. The noise as a function of signal intensity can then be written as:

$$\beta I+(c_{pr}I)^2=\sigma_I^2 \qquad \text{(SI-4)}$$

Where c_{pr} is the flicker factor. The β and c_{pr} is determined by fitting the square of the noise amplitude as a function of signal intensity with a function of type ax^2+bx. The coefficients β and c_{pr} were determined to 22.64 and 0.102 respectively.